Journal of Palaeogeography, 2024, 13(1): 116–126 (00323)

Available online at www.sciencedirect.com

ScienceDirect

journal homepage: http://www.journals.elsevier.com/journal-of-palaeogeography/

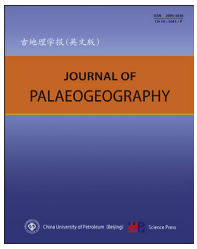


Sedimentary geochemistry

# Power-law patterns in the Phanerozoic sedimentary records of carbon, oxygen, sulfur, and strontium isotopes

*Haitao Shang*

*Institute of Ecology and Evolution, University of Oregon, Eugene, OR, 97403, USA*

**Abstract** Power-law patterns appear in a variety of natural systems on the modern Earth; nevertheless, whether such behaviors appeared in the deep-time environment has rarely been studied. Isotopic records in sedimentary rocks, which are widely used to reconstruct the geological/geochemical conditions in paleoenvironments and the evolutionary trajectories of biogeochemical cycles, offer an opportunity to investigate power laws in ancient geological systems. In this study, I focus on the Phanerozoic sedimentary records of carbon, oxygen, sulfur, and strontium isotopes, which have well documented and extraordinarily comprehensive datasets. I perform statistical analyses on these datasets and show that the variations in the sedimentary records of the four isotopes exhibit power-law behaviors. The exponents of these power laws range between 2.2 and 2.9; this narrow interval indicates that the variations in carbon, oxygen, sulfur, and strontium isotopes likely belong to the same universality class, suggesting that these systematic power-law patterns are governed by universal, scale-free mechanisms. I then derive a general form for these power laws from a minimalistic model based on basic physical principles and geosystem-specific assumptions, which provides an interpretation for the power-law patterns from the perspective of thermodynamics. The fundamental mechanisms regulating such patterns might have been ubiquitous in paleoenvironments, implying that similar power-law behaviors may exist in the sedimentary records of other isotopes.

**Keywords** Power laws, Phanerozoic sedimentary records, Carbon isotope ($\delta^{13}C$), Oxygen isotope ($\delta^{18}O$), Sulfur isotope ($\delta^{34}S$), Strontium isotope ($^{87}Sr/^{86}Sr$)



Received 25 June 2023; revised 5 November 2023; accepted 27 November 2023; available online 28 November 2023

E-mail address: htshang.research@gmail.com.

Peer review under responsibility of China University of Petroleum (Beijing).

https://doi.org/10.1016/j.jop.2023.11.003

## 1. Introduction

The Phanerozoic Eon witnessed a variety of spatial and temporal changes in the geological system. The fingerprints that isotopes left in sedimentary records provide a window through which to reconstruct environmental conditions on the ancient Earth and to investigate significant changes in biogeochemical cycles (Hoefs, 1997; Michener and Lajtha, 2007). Among the isotopes that are used as geological/geochemical proxies for paleoenvironments, the isotopes of four elements — carbon ($\delta^{13}C$), oxygen ($\delta^{18}O$), sulfur ($\delta^{34}S$), and strontium ($^{87}Sr/^{86}Sr$) — have rather long histories of application in geosciences and have been widely used to explore fundamental geological questions. After extensive measurements of $\delta^{13}C$, $\delta^{18}O$, $\delta^{34}S$, and $^{87}Sr/^{86}Sr$ in a variety of geological settings in the past several decades, we have well documented datasets for these four isotopes, allowing us to investigate their evolutionary trajectories and dynamical properties over geologic time.

Carbon, oxygen, sulfur, and strontium isotopes serve as proxies for different aspects of the environmental conditions or biogeochemical cycles. Fluctuations in carbon isotope records reflect the variations in the exchange between the isotopically heavy inorganic and isotopically light organic reservoirs (Hayes and Waldbauer, 2006; Cramer and Jarvis, 2020). Oxygen isotopes, which are influenced by and covary with temperature, have recorded climate changes through geologic time (Veizer and Prokoph, 2015; Grossman and Joachimski, 2020). The variations in sulfur isotopes are linked to marine sulfate concentrations via microbial metabolisms, especially microbial sulfate reduction, and thus offer an avenue to study seawater sulfate changes throughout Earth history (Paytan *et al.*, 2020; Present *et al.*, 2020). Strontium isotopes are tied to the balance between the fluxes from the continental and mantle reservoirs and therefore are widely used to reconstruct weathering rates and tectonic events in deep time (Prokoph *et al.*, 2008; McArthur *et al.*, 2020).

The power law is a functional relation between two variables in which one variable changes as a power of the other. Generally, power laws are expressed as $y \propto x^{-\alpha}$, where $x$ and $y$ are two variables and $\alpha > 0$ is usually referred to as the power-law exponent. On a double logarithmic plot, they are written as $\log_{10} y \propto -\alpha \log_{10} x$, which is a straight line and implies that the underlying regularity of this relation is independent of specific scales (Schroeder, 2009; Bak, 2013). Although power laws are commonly taken as hints of fundamental mechanisms behind the observed data, the specific mechanisms of many power-law behaviors remain unknown (Schroeder, 2009; Bak, 2013). Power laws are ubiquitous in the modern Earth system (Schroeder, 2009; Bak, 2013); for example, the distribution of the size of lakes and faults (Mandelbrot, 1982; Scholz and Mandelbrot, 1989), the frequency versus magnitude of earthquakes and volcanic eruptions (Scholz and Mandelbrot, 1989; Mega *et al.*, 2003), and the degradation rate constant versus age of organic matter in natural ecosystems (Middelburg, 1989; Katsev and Crowe, 2015; Shang, 2023a) have been shown to exhibit power laws. Whether such behaviors existed in the deep-time geological system, however, has rarely been studied, partially due to the sparsity and limited availability of datasets on a majority of geological/geochemical quantities characterizing paleoenvironments. After all, investigating power-law patterns, which usually spans several orders of magnitude, requires large and diverse datasets that consist of data points representing enormously small and extremely large events. The $\delta^{13}C$, $\delta^{18}O$, $\delta^{34}S$, and $^{87}Sr/^{86}Sr$, which have extraordinarily comprehensive datasets in deep time, especially during the Phanerozoic Eon, offer an opportunity to explore power-law patterns on the ancient Earth.

Here, I investigate the variations in the Phanerozoic sedimentary records of $\delta^{13}C$, $\delta^{18}O$, $\delta^{34}S$, and $^{87}Sr/^{86}Sr$ and show that they exhibit power-law behaviors. The exponents of these power laws vary between 2.2 and 2.9 (with a mean of 2.58 and standard deviation of 0.23); this small range of power-law exponents suggests that variations in these four isotopes likely belong to the same universality class, implying that the systematic power laws for these four isotopes may be regulated by universal and scale-free mechanisms. To explore the underlying mechanisms, I derive a general form of these power laws with some basic physical principles and geosystem-specific assumptions, which offers an interpretation for the origin of such patterns from the perspective of thermodynamics. Due to the limited availability of datasets on other isotopes, I only focus on the power-law patterns for carbon, oxygen, sulfur, and strontium isotopes in this study. However, the fundamental principles governing such behaviors should have been universal, indicating that the sedimentary records of other isotopes might also exhibited power-law patterns in deep time.

## 2. Material and methods

### 2.1. Data processing and fitting

The dataset on $\delta^{13}C$ is from Cramer and Jarvis (2020) and Westerhold *et al.* (2020), the dataset on $\delta^{18}O$ is from Veizer and Prokoph (2015) and Westerhold *et al.* (2020), the dataset on $\delta^{34}S$ is from Present *et al.* (2020), and the dataset on $^{87}Sr/^{86}Sr$ is from Prokoph *et al.* (2008). Power laws generally span several orders of magnitude; I perform spline interpolations to obtain data points at fine timescales (Friedman, 1991; De Boor, 2001; Ruppert, 2002). Spline interpolations have been shown to be effective for fitting the sedimentary records of these four isotopes at geologic timescales (Howarth and McArthur, 1997; Kasting *et al.*, 2006; Wu *et al.*, 2010; Ovtcharova *et al.*, 2015). Here I interpolate each dataset with different types of splines including the smoothing (De Boor, 2001), regression (Friedman, 1991), and penalized (Ruppert, 2002) splines and find that penalized splines generate the best-fitting curve (based on the residuals) for the four datasets. I calculate the data value at every 0.05 million years with the best-fitting penalized splines.

I denote the time series of an isotope (*i.e.*, data points in an isotopic dataset) as $\{\xi_i\}$, where $\xi_i$ is the mean of data at time point $i$. For each dataset, I take the difference between the data values at every two consecutive time points (*i.e.*, $\xi_i$ and $\xi_{i+1}$) and denote this variation at time point $i$ as $\theta_i = \xi_{i+1} - \xi_i$. The variations (*i.e.*, $\theta_i$'s) in the time series $\{\xi_i\}$ are classified into three categories: decrease (D), increase (I), and change (C). Logarithms of negative values are undefined; I denote the absolute values of variations in these three categories by $|D| = \{|\theta_i| : \theta_i < 0\}$, $|I| = \{|\theta_i| : \theta_i > 0\}$, and $|C| = \{|\theta_i| : \theta_i \neq 0\}$, and use data points in these three categories to investigate power laws. Obviously, $|C|$ is the union of $|D|$ and $|I|$: $|C| = |D| \cup |I|$. I do not consider $\theta_i = 0$ here not only since a zero value indicates no variation but also because the logarithm of zero is mathematically undefined.

The absolute values of variations (*i.e.*, $|\theta_i|$'s defined above) in each category (*i.e.*, $|D|$, $|I|$, and $|C|$) are grouped into bins. The optimal number of bins, $N_B$, is determined using Sturges' Rule: $N_B = \log_2(N_D)+1$, where $N_D$ is the number of data points in a dataset, and the number of data (*i.e.*, counts) in the $k$-th bin is denoted as $N_k$. An intriguing feature of power-law distributions is their right tails, where large values of random variables appear (Clauset *et al.*, 2009; Alstott *et al.*, 2014). The initial data values on the left side sometimes do not follow a power-law pattern and should not be included when fitting power laws (Clauset *et al.*, 2009; Alstott *et al.*, 2014). To determine where to truncate the set of counts $\{N_k\}$, one needs to identify the data point beyond which the power-law relation appears; this truncation point is henceforth denoted as $N_{min}$. A common approach to identify $N_{min}$ is establishing a power-law fit starting from each individual data point in $\{N_k\}$ and then choosing the point generating the minimum value for the distance between the fit and the data (Clauset *et al.*, 2009; Alstott *et al.*, 2014). The power law best fitting the truncated dataset with $N_{min}$ as the initial point therefore is the optimal power law for the data.

### 2.2. Goodness-of-fit tests

Testing the goodness of fit of a power law is an indispensable step before concluding that this power law serves an adequate description of the data. In this study, I employ two conventional goodness-of-fit tests, the Kolmogorov–Smirnov (KS) test (Massey, 1951) and the Cramér-von Mises two-sample test (Anderson, 1962), to check whether the estimated power-law formula fit the data well. The KS statistic is defined as the maximum distance between the cumulative distribution functions (CDFs) (Massey, 1951): $D_{KS} = \sup |F_{data}(\theta_i) - F_0(\theta_i)|$, where $F_{data}$ is the CDF of the observed data and $F_0$ is the CDF of the estimated power-law distribution best fitting the observed data. The CM two-sample test is based on the following statistic (Anderson, 1962): $D_{CM} = \frac{m\times n}{(m+n)^2}\left(\sum_{i=1}^{m}[F_{data}(\theta_i) - F_0(\theta_i)]^2 + \sum_{j=1}^{n}[F_{data}(\theta_j') - F_0(\theta_j')]^2\right)$, where $\{\theta_i\}_{i=1}^{m}$ and $\{\theta_j'\}_{j=1}^{n}$ are two sample sets that are independently drawn from two distributions with two CDFs, $F_{data}$ and $F_0$, respectively; the definitions of $F_{data}$ and $F_0$ in the statistic $D_{CM}$ are the same as those in the statistic $D_{KS}$. In this study, I test the null hypothesis, $H_0 : F_{data} = F_0$, against the two-sided alternative, $H_1 : F_{data} \neq F_0$, and set the critical $p$-value to 0.05. When $p \leq 0.05$, one rejects the null hypothesis and concludes that $F_{data}$ is unlikely to be the same as $F_0$; however, when $p > 0.05$, one fails to reject the null hypothesis and concludes that $F_{data}$ is very likely to be the same as $F_0$.

### 2.3. Likelihood-ratio tests

The power law is not the only distribution that is able to result in a straight line on a log–log plot; other heavy-tailed distributions, such as stretched exponential and lognormal distributions, can generate datasets with distributions that are close to power

laws. To test if the best-fitting power laws fit the given datasets better than other heavy-tailed distributions, I conduct the likelihood-ratio test (Clauset *et al.*, 2009): $\mathcal{L}R = \log(\mathcal{L}_{PL} / \mathcal{L}_{HT})$, where $\mathcal{L}_{PL}$ is the likelihood, fitted using the above procedure, under the hypothesis of a power-law distribution; while $\mathcal{L}_{HT}$ is the likelihood, fitted using maximum likelihood estimation, under the hypothesis of an alternative heavy-tailed distribution. When $\mathcal{L}R$ is greater than zero, the best-fitting power law performs better than the alternative heavy-tailed distribution; however, when $\mathcal{L}R$ is less than zero, the alternative heavy-tailed distribution outperforms the best-fitting power law. I standardize $\mathcal{L}R$ with the standard deviation to correct for random fluctuations (Vuong, 1989; Clauset *et al.*, 2009) and get a *p*-value for justifying whether the sign of $\mathcal{L}R$ is statistically significant. I set the significance level for the *p*-value to 0.05. When the *p*-value is less than 0.05, I conclude that one distribution outperforms the other for the given dataset; however, when the *p*-value is greater than or equal to 0.05, the likelihood-ratio test is not conclusive because the sign of $\mathcal{L}R$ may originate from chance fluctuations.

## 3. Results and discussion

### 3.1. Power laws in Phanerozoic isotopic records

Fig. 1 illustrates the variations (*i.e.*, $\theta_i$'s) in (A) $\delta^{13}C$, (B) $\delta^{18}O$, (C) $\delta^{34}S$, and (D) $^{87}Sr/^{86}Sr$ during the Phanerozoic Eon. I classify the variations in each of the four isotopes into three categories: decrease ( $|D|$ ), increase ( $|I|$ ), and change ( $|C|$ ), which are defined in Section 2.1. Fig. 2 shows power-law patterns in these three categories of variations in (A–C) $\delta^{13}C$, (D–F) $\delta^{18}O$, (G–I) $\delta^{34}S$, and (J–L) $^{87}Sr/^{86}Sr$. The fitted mathematical expressions of these power laws and their coefficients of determination ($R^2$'s) and root mean square errors (RMSEs) are presented in Table 1. To justify the goodness of fit of these power laws, I perform the KS and CM tests and calculate their *p*-values, which are denoted by $p_{KS}$ and $p_{CM}$, respectively. The results (Table 1) show that the *p*-values of these tests are all much greater than the critical threshold of 0.05 (Section 2.2), suggesting that the mathematical formulas of the power laws in Table 1 fit the data well. Although a straight line on a log–log plot is a key characteristic of power-law patterns, it does not guarantee that the fitted data are from a power-law distribution because other heavy-tailed processes, such as stretched exponential and lognormal distributions, are able to generate data that have distributions similar to power laws due to random fluctuations (Clauset *et al.*, 2009; Alstott *et al.*, 2014). To test whether the best-fitting power laws in this study outperform other heavy-tailed distributions, I perform the likelihood-ratio test (Section 2.3). The results suggest that the best-fitting power laws presented in Table 1 and Fig. 2 fit the datasets better than exponential, stretched exponential, and lognormal distributions. In the next section, I show that a general form of the power-law relations presented here (Table 1 and Fig. 2) can be derived from a conceptual model with basic principles of statistical mechanics and some geosystem-specific assumptions.

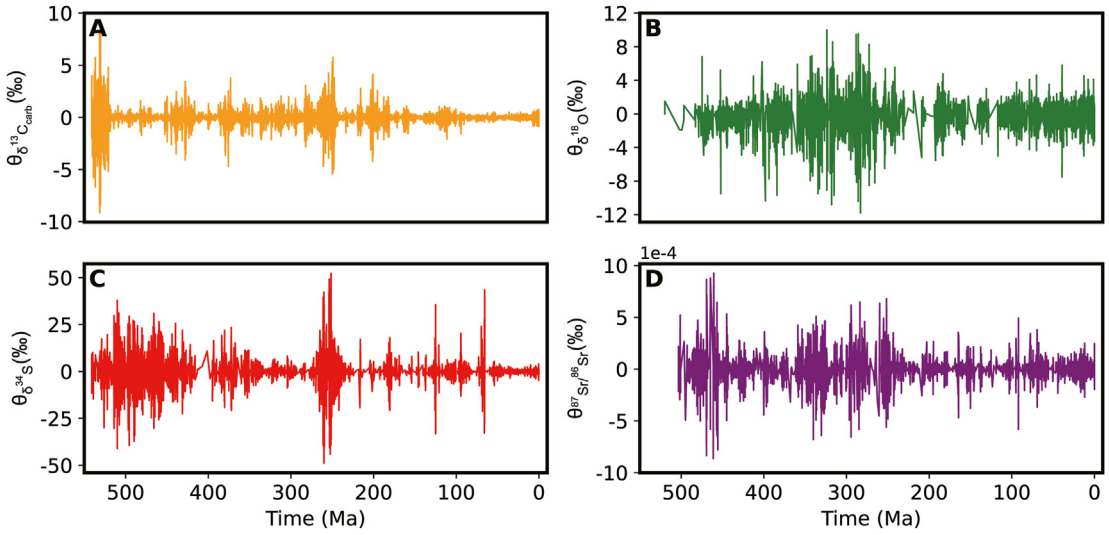


**Fig. 1** Time series of the variations (*i.e.*, $\theta_i$'s defined in Section 2.1) in **(A)** $\delta^{13}C$ (orange), **(B)** $\delta^{18}O$ (green), **(C)** $\delta^{34}S$ (red), and **(D)** $^{87}Sr/^{86}Sr$ (purple) during the Phanerozoic Eon.

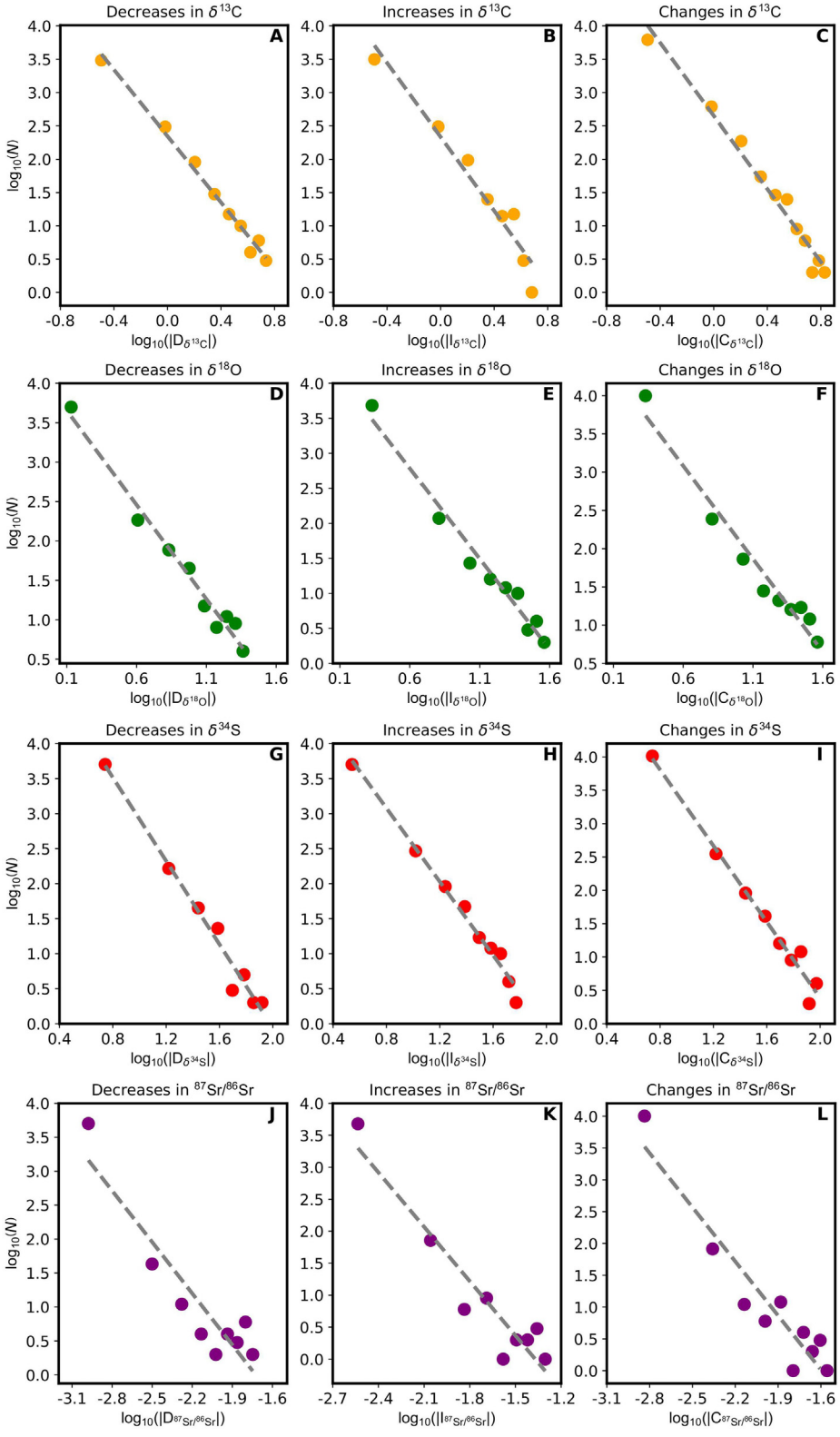


**Fig. 2** Power laws of the decreases (|D|), increases (|I|), and changes (|C|) in the Phanerozoic sedimentary records of **(A—C)** $\delta^{13}C$, **(D—F)** $\delta^{18}O$, **(G—I)** $\delta^{34}S$, and **(J—L)** $^{87}Sr/^{86}Sr$. Orange, green, red, and purple circles represent counts (*i.e.*, *N*'s) versus variations (*i.e.*, $|\theta_i|$'s defined in Section 2.1) of $\delta^{13}C$, $\delta^{18}O$, $\delta^{34}S$, and $^{87}Sr/^{86}Sr$, respectively. Grey dashed lines are the least-squares fitting of data on log—log plots. The mathematical expressions of power laws, the $R^2$'s and RMSEs of least-squares-fitting lines, and the KS and CM *p*-values for goodness-of-fit tests are provided in Table 1.

**Table 1** Power laws of the decreases (|D|), increases (|I|), and changes (|C|) in the Phanerozoic records of $\delta^{13}C$, $\delta^{18}O$, $\delta^{34}S$, and $^{87}Sr/^{86}Sr$. The $R^2$, RMSE, $p_{KS}$, and $p_{CM}$ represent the coefficient of determination, root mean square error, the *p*-value of the KS test, and the *p*-value of the CM test, respectively, of the least-squares fitting on log—log plots.

| Variable | Category | Best-fitting power law | $R^2$ | RMSE | $p_{KS}$ | $p_{CM}$ |
|---|---|---|---|---|---|---|
| $\delta^{13}C$ | Decreases in $\delta^{13}C$ | $N \sim \lvert D_{\delta^{13}C} \rvert^{-2.33}$ | 0.95 | 0.13 | 1.00 | 1.00 |
| | Increases in $\delta^{13}C$ | $N \sim \lvert I_{\delta^{13}C} \rvert^{-2.74}$ | 0.96 | 0.23 | 1.00 | 1.00 |
| | Changes in $\delta^{13}C$ | $N \sim \lvert C_{\delta^{13}C} \rvert^{-2.71}$ | 0.95 | 0.18 | 1.00 | 1.00 |
| $\delta^{18}O$ | Decreases in $\delta^{18}O$ | $N \sim \lvert D_{\delta^{18}O} \rvert^{-2.36}$ | 0.98 | 0.13 | 1.00 | 1.00 |
| | Increases in $\delta^{18}O$ | $N \sim \lvert I_{\delta^{18}O} \rvert^{-2.44}$ | 0.96 | 0.17 | 1.00 | 0.99 |
| | Changes in $\delta^{18}O$ | $N \sim \lvert C_{\delta^{18}O} \rvert^{-2.25}$ | 0.97 | 0.15 | 0.98 | 0.91 |
| $\delta^{34}S$ | Decreases in $\delta^{34}S$ | $N \sim \lvert D_{\delta^{34}S} \rvert^{-2.87}$ | 0.94 | 0.17 | 0.99 | 0.99 |
| | Increases in $\delta^{34}S$ | $N \sim \lvert I_{\delta^{34}S} \rvert^{-2.54}$ | 0.97 | 0.12 | 1.00 | 1.00 |
| | Changes in $\delta^{34}S$ | $N \sim \lvert C_{\delta^{34}S} \rvert^{-2.82}$ | 0.97 | 0.15 | 0.98 | 0.91 |
| $^{87}Sr/^{86}Sr$ | Decreases in $^{87}Sr/^{86}Sr$ | $N \sim \lvert D_{^{87}Sr/^{86}Sr} \rvert^{-2.31}$ | 0.83 | 0.27 | 0.97 | 0.92 |
| | Increases in $^{87}Sr/^{86}Sr$ | $N \sim \lvert I_{^{87}Sr/^{86}Sr} \rvert^{-2.86}$ | 0.82 | 0.25 | 0.99 | 0.66 |
| | Changes in $^{87}Sr/^{86}Sr$ | $N \sim \lvert C_{^{87}Sr/^{86}Sr} \rvert^{-2.84}$ | 0.89 | 0.29 | 1.00 | 0.99 |

### 3.2. Derivation of the general form of power laws in isotopic records

The values of $\delta^{13}C$, $\delta^{18}O$, $\delta^{34}S$, and $^{87}Sr/^{86}Sr$ manifest different aspects of planetary-scale biogeochemical cycles; their variations thus should characterize the changes in the states of the global biogeosystem. As mentioned in Section 2.1, I denote the realizations of an isotopic value at time step $i$ by $\xi_i$. The entropy of the biogeosystem at the state corresponding to $\xi_i$ is then expressed as $S(\xi_i) = -\log p(\xi_i)$, where $p(\xi_i)$ is the probability that the realization $\xi_i$ occurs and $S(\xi_i)$ characterizes the extent to which the system at the state corresponding to $\xi_i$ deviates from the equilibrium. I denote the difference between these two consecutive realizations by $\Theta_i = \xi_{i+1} - \xi_i$, where $i \in I$ and $I$ is the index set of all realizations. Here, I denote the difference between $\xi_{i+1}$ and $\xi_i$ by $\Theta_i$ instead of $\theta_i$ as defined in Section 2.1 because, for simplicity, I assume that $\xi_i < \xi_{i+1}$ in the following derivation so that $\Theta_i > 0$ holds for all $i \in I$ and thus $\log \Theta_i$ is always mathematically well-defined. For the case of $\Theta_i < 0$, the same general form of power laws (*i.e.*, $N(\Theta_i) \sim |\Theta_i|^{-\alpha}$) can be obtained by replacing $\Theta_i$ with its absolute value ($|\Theta_i|$) (refer to |D|, |I|, and |C| defined in Section 2.1). The case of $\Theta_i = 0$ is not considered here because the logarithm of zero is not defined in mathematics (Section 2.1).

When the system switches from state $\xi_i$ to state $\xi_{i+1}$, the change in entropy is expressed as $\Delta S_i = S(\xi_{\xi_{i+1}}) - S(\xi_i)$. According to the additivity of entropy (Skilling, 1989; Almeida, 2003), I obtain $\Delta S_i = S(\xi_{i+1} - \xi_i) = -\log p(\Theta_i)$. For simplicity, I henceforth write $p(\Theta_i)$ as $p_i$. The average of $\Delta S_i$ over all $i \in I$ then can be expressed as $\mathbb{E}(\Delta S_i) = -\sum_{i \in I} p_i \cdot \log p_i$, where $\mathbb{E}(\cdot)$ is the expectation value of a variable. Moreover, as a probability density, the summation of $p_i$ over $i \in I$ satisfies $\sum_{i \in I} p_i = 1$. The Gaia hypothesis suggests that the geological and biological processes on Earth's surface are intertwined, driving the biogeosystem to a stable world (Lenton, 1998; Lovelock, 2000; Lenton and Watson, 2013). Under a variety of feedback mechanisms, variations in the Earth system are balanced, maintaining Earth's surface environment and its components at steady states over geologic timescales (Lenton, 1998; Lovelock, 2000; Lenton and Watson, 2013). The structures of complex systems, such as Earth's surface environment, usually lie at certain intermediate levels between perfect order and perfect disorder (Anderson, 1972; Prigogine, 1980; Bak, 2013); the order of magnitude of quantities may better characterize the variability and complexity of the global biogeosystem than their precise values. I denote the order of magnitude of the variation in isotopic values at time step $i$ by $\mathcal{O}(\Theta_i) \sim \log \Theta_i$. Based on the steady-state evolution of the global biogeosystem proposed by the Gaia hypothesis (Lenton, 1998; Lovelock, 2000; Lenton and Watson, 2013), I assume that the average change in the magnitudes of variations in isotopic values is a constant: $\sum_{i \in I} p_i \cdot \log \Theta_i \simeq \psi$, where $\psi$ is a constant.

Although geological and biological feedback mechanisms maintain the habitability of Earth's surface environment (Lenton, 1998; Lovelock, 2000; Lenton and Watson, 2013), individual physical and biological processes usually are dissipative and tend to force the geological system and its components away from steady states, resulting in fluctuations around equilibria (Kleidon, 2010; Vallino and Algar, 2016). In statistical mechanics, the well-known maximum entropy production (MEP) principle suggests that a nonlinear system possessing a high degree of freedom, such as the Earth system, evolves through the trajectories that maximize the change of entropy in the phase space

(Kleidon and Lorenz, 2005; Martyushev, 2010). Based on the MEP principle, I apply the method of Lagrange multipliers (Jaynes, 1957) to compute the maximum of the average change in entropy defined above, that is, the maximum of $\mathbb{E}(\Delta S_i) = -\sum_{i\in I} p_i \cdot \log p_i$. Under the constraints of (1) the normalization condition (*i.e.*, $\sum_{i\in I} p_i = 1$) and (2) the assumption that the average change in the magnitudes of variations in isotopic values is maintained constant (*i.e.*, $\sum_{i\in I} p_i \cdot \log \Theta_i \simeq \psi$), I write the following Lagrangian: $\mathcal{L} = -\sum_{i\in I} p_i \cdot \log p_i + \eta\left(1 - \sum_{i\in I} p_i\right) + \alpha\left(\psi - \sum_{i\in I} p_i \cdot \log \Theta_i\right)$, where the two positive numbers, $\eta$ and $\alpha$, are Lagrange multipliers. Taking the derivative of $\mathcal{L}$ with respect to $p_i$, I obtain $\partial\mathcal{L}/\partial p_i = -(\log p_i + 1) - \eta - \alpha \log \Theta_i$. When $\partial\mathcal{L}/\partial p_i = 0$, I obtain $p_i = \exp[-(\eta + 1)] \cdot \Theta_i^{-\alpha}$. If one takes $\xi$ measurements, the number of variations with the value $\Theta_i$ is $N(\Theta_i) = \xi \cdot p_i$. The relation between $N(\Theta_i)$ and $\Theta_i$ then follows $N(\Theta_i) \sim \Theta_i^{-\alpha}$, which is a general form of the power laws presented in Table 1 and Fig. 2.

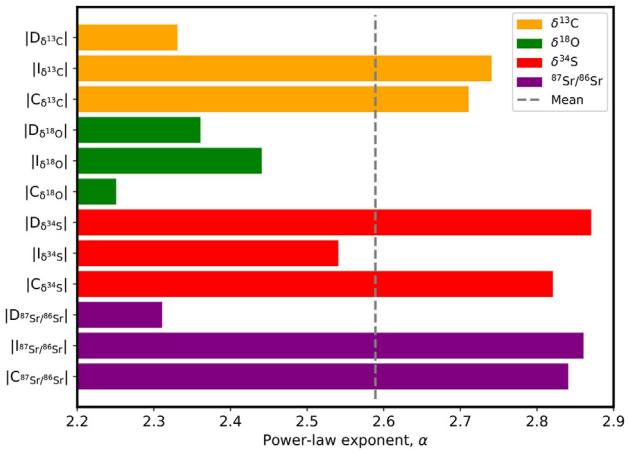


**Fig. 3** Power-law exponents ($\alpha$'s) for the three categories of variations (*i.e.*, decrease |D|, increase |I|, and change |C|) in the Phanerozoic records of carbon ($\delta^{13}C$), oxygen ($\delta^{18}O$), sulfur ($\delta^{34}S$), and strontium ($^{87}Sr/^{86}Sr$) isotopes. Orange, green, red, and purple bars represent the power-law exponents for the variations in $\delta^{13}C$, $\delta^{18}O$, $\delta^{34}S$, and $^{87}Sr/^{86}Sr$, respectively. Vertical grey dashed line shows the mean of the exponents of all power laws for the four isotopes.

### 3.3. *Geological implications*

The systematic power-law patterns appearing in the variations of carbon, oxygen, sulfur, and strontium isotopes (Table 1 and Fig. 2) have two straightforward implications: (1) large variations in these isotopic records are much rarer than small ones, and (2) these variations are likely to have been regulated by scale-free mechanisms (Schroeder, 2009; Bak, 2013). In statistical mechanics, the specific values of power-law exponents (*i.e.*, $\alpha$'s introduced in **Section 1**) are used as a key indicator of systems' dynamical properties. Fig. 3 summarizes the exponents of power laws for the variations in carbon (orange bars), oxygen (green bars), sulfur (red bars), and strontium (purple bars) isotopes. The mean value and standard deviation of these exponents are $\mu_\alpha \simeq 2.58$ (vertical grey dashed line in Fig. 3) and $\sigma_\alpha \simeq 0.23$, respectively. The coefficient of variation (*i.e.*, the ratio of the standard deviation to the mean) equals $\sigma_\alpha/\mu_\alpha \simeq 8.91\,\%$, indicating that the deviations of these exponents are very small relative to their mean. From the perspective of nonlinear dynamics, systems having identical power-law exponents are in the same universality class (Kadanoff, 1990; Stanley *et al.*, 2000). The rather small range of the exponents shown in Fig. 3 implies that the variations of carbon, oxygen, sulfur, and strontium isotopes in the Phanerozoic sedimentary records may belong to the same universality class, suggesting that these power-law patterns are likely to be regulated by certain fundamental and universal mechanisms. However, like many complex systems possessing power-law patterns, the underlying mechanisms responsible for the power laws shown in this study (Table 1 and Fig. 2) remain unclear.

In statistical mechanics, power-law patterns are commonly attributed to self-organized criticality (SOC), which refers to the phenomenon that the internal interactions of a large system self-organize it into states at which power-law behaviors appear (Bak *et al.*, 1987, 1988). Nevertheless, power-law patterns, as an emergent property of SOC, do not necessarily originate from the latter (Hergarten, 2002; Solow, 2005; Marković and Gros, 2014); whether the power laws presented here (Table 1 and Fig. 2) are related to SOC remains unknown. In this work, I derive a general form of these power laws with a simple model based on some physical principles and geosystem-specific assumptions. This model, however, does not provide interpretations for the specific values of the power-law exponents; more universal and fundamental theories are expected to be suggested by future work to shed light on the geological and biological mechanisms responsible for these power-law patterns.

The extraordinarily large variations in deep-time sedimentary records of isotopes, which appear on the right tails of the power-law patterns in Fig. 2, have attracted much attention in geological and geochemical studies and are considered to manifest extreme events in the deep-time biogeosystem. For

instance, the Lomagundi-Jatuli event (the most protracted positive excursion of the carbon isotope in Earth history) (Grotzinger *et al.*, 2011) and Shuram-Wonoka excursion (the deepest negative excursion of the carbon isotope in Earth history) (Husson *et al.*, 2015) link to two significant transitions in the evolution of Earth's oxygen cycle: the Great Oxygenation Event (~2400—2300 Ma) and the Neoproterozoic Oxygenation Event (~850—540 Ma) (Lyons *et al.*, 2014; Canfield, 2016), respectively. Another example is the prominent excursions of carbon and oxygen isotopes that simultaneously occurred at the boundary between the Paleocene and Eocene epochs (~56 Ma), also referred to as the Paleocene—Eocene Thermal Maximum event, indicating a period of abrupt and remarkable global warming (McInerney and Wing, 2011; Bowen *et al.*, 2015). These extreme events contribute to the right tails of the power laws (Fig. 2) and are likely to have been triggered by the complex feedback mechanisms in Earth's biogeochemical cycles (McInerney and Wing, 2011; Shang *et al.*, 2022; Tierney *et al.*, 2022; Shang, 2023b). However, the power-law behaviors in other deep-time geological/geochemical datasets may remain obscure because data points manifesting extreme events might have been treated as outliers and removed in the initial stage of statistical analyses. Therefore, careful assessments of seemingly abnormal data points in geological/geochemical measurements (prior to being discarded) are crucial for revealing the dynamical patterns (such as power laws) and their underlying mechanisms in paleoenvironments.

Due to the sparsity and limited availability of datasets on other isotopes, I investigate only the power laws for carbon, oxygen, sulfur, and strontium isotopes, which have comprehensive datasets after extensive studies in the past decades. Power-law patterns, however, probably exist in other isotopes characterizing deep-time physical/chemical conditions and biogeochemical cycles, such as lithium ($\delta^7$Li) (Penniston-Dorland *et al.*, 2017; Kalderon-Asael *et al.*, 2021), calcium ($\delta^{44/40}$ Ca) (Farkaš *et al.*, 2007; Blättler *et al.*, 2012), and uranium ($\delta^{234}$U, $\delta^{235}$U, and $\delta^{238}$U) (Zhang *et al.*, 2020; Kipp *et al.*, 2022) isotopes. Future measurements of Phanerozoic sedimentary records of these isotopes at the global scale could examine whether power-law behaviors also appear in their variations. Moreover, the fundamental physics governing the Phanerozoic Earth system should have been the same during the Precambrian, indicating that the isotopic records and other quantities characterizing geological changes (*e.g.*, atmospheric $CO_2$ level and surface temperature) might have exhibited power-law patterns on the Precambrian Earth as well. These power laws can be used as hints to decipher the underlying mechanisms responsible for the planetary-scale dynamics of the Earth system over geologic time.

## Funding

This work received no financial support from any project or organization.

## Availability of data and materials

Data supporting the findings of this study are available upon request from the author.

## Authors' contributions

H.S. conceived the project, performed the research, and wrote the manuscript. The author read and approved the final version of the manuscript.

### Conflicts of interest

The author declares no known competing financial interests or personal relationships that could have appeared to influence the work reported in this paper.

## Acknowledgements

I thank the Associate Editor-in-Chief Prof. Santanu Banerjee for valuable suggestions and securing reviewers for the manuscript and anonymous reviewers for thoughtful and constructive comments.

## References

Almeida, M.P., 2003. Thermodynamical entropy (and its additivity) within generalized thermodynamics. *Physica A: Statistical Mechanics and its Applications*, 325, 426—438. https://doi.org/10.1016/S0378-4371(03)00262-0.

Alstott, J., Bullmore, E., Plenz, D., 2014. Powerlaw: A Python package for analysis of heavy-tailed distributions. *PLOS ONE*, 9, e85777. https://doi.org/10.1371/journal.pone.0085777.

Anderson, P.W., 1972. More is different: Broken symmetry and the nature of the hierarchical structure of science. *Science*, 177, 393—396. https://doi.org/10.1126/science.177.4047.393.

Anderson, T.W., 1962. On the distribution of the Two-Sample Cramér-von Mises Criterion. *The Annals of Mathematical Statistics*, 33, 1148—1159. https://doi.org/10.1214/aoms/1177704477.

Bak, P., 2013. *How Nature Works: The Science of Self-Organized Criticality*. Springer, New York.

Bak, P., Tang, C., Wiesenfeld, K., 1988. Self-organized criticality. *Physical Review A*, 38, 364—374. https://doi.org/10.1103/PhysRevA.38.364.

Bak, P., Tang, C., Wiesenfeld, K., 1987. Self-organized criticality: An explanation of the 1/f noise. *Physical Review Letters*, 59, 381—384. https://doi.org/10.1103/PhysRevLett.59.381.

Blättler, C.L., Henderson, G.M., Jenkyns, H.C., 2012. Explaining the Phanerozoic Ca isotope history of seawater. *Geology*, 40, 843—846. https://doi.org/10.1130/G33191.1.

Bowen, G.J., Maibauer, B.J., Kraus, M.J., Röhl, U., Westerhold, T., Steimke, A., Gingerich, P.D., Wing, S.L., Clyde, W.C., 2015. Two massive, rapid releases of carbon during the onset of the Paleocene—Eocene Thermal Maximum. *Nature Geoscience*, 8, 44—47. https://doi.org/10.1038/ngeo2316.

Canfield, D.E., 2016. *Oxygen: A Four Billion Year History*. Princeton University Press, Princeton. https://doi.org/10.1515/9781400849888.

Clauset, A., Shalizi, C.R., Newman, M.E.J., 2009. Power-law distributions in empirical data. *SIAM Review*, 51, 661—703. https://doi.org/10.1137/070710111.

Cramer, B.D., Jarvis, I., 2020. Carbon Isotope Stratigraphy. In: *Geologic Time Scale 2020*. Elsevier, pp. 309—343. https://doi.org/10.1016/B978-0-12-824360-2.00011-5.

De Boor, C., 2001. *A Practical Guide to Splines*. Springer, New York.

Farkaš, J., Böhm, F., Wallmann, K., Blenkinsop, J., Eisenhauer, A., Van Geldern, R., Munnecke, A., Voigt, S., Veizer, J., 2007. Calcium isotope record of Phanerozoic oceans: Implications for chemical evolution of seawater and its causative mechanisms. *Geochimica et Cosmochimica Acta*, 71, 5117—5134. https://doi.org/10.1016/j.gca.2007.09.004.

Friedman, J.H., 1991. Multivariate adaptive regression splines. *Annals of Statistics*, 19, 1—67. https://doi.org/10.1214/aos/1176347963.

Grossman, E.L., Joachimski, M.M., 2020. Oxygen Isotope Stratigraphy. In: *Geologic Time Scale 2020*. Elsevier, pp. 279—307. https://doi.org/10.1016/B978-0-12-824360-2.00010-3.

Grotzinger, J.P., Fike, D.A., Fischer, W.W., 2011. Enigmatic origin of the largest-known carbon isotope excursion in Earth's history. *Nature Geoscience*, 4, 285—292. https://doi.org/10.1038/ngeo1138.

Hayes, J.M., Waldbauer, J.R., 2006. The carbon cycle and associated redox processes through time. *Philosophical Transactions of the Royal Society B: Biological Sciences*, 361, 931—950. https://doi.org/10.1098/rstb.2006.1840.

Hergarten, S., 2002. *Self-Organized Criticality in Earth Systems*. Springer, Heidelberg. https://doi.org/10.1007/978-3-662-04390-5.

Hoefs, J., 1997. *Stable Isotope Geochemistry*. Springer, Heidelberg. https://doi.org/10.1007/978-3-662-03377-7.

Howarth, R.J., McArthur, J.M., 1997. Statistics for strontium isotope stratigraphy: A robust LOWESS fit to the marine Sr-isotope curve for 0 to 206 Ma, with look-up table for derivation of numeric age. *The Journal of Geology*, 105, 441—456. https://doi.org/10.1086/515938.

Husson, J.M., Maloof, A.C., Schoene, B., Chen, C.Y., Higgins, J.A., 2015. Stratigraphic expression of Earth's deepest $\delta^{13}C$ excursion in the Wonoka Formation of South Australia. *American Journal of Science*, 315, 1—45. https://doi.org/10.2475/01.2015.01.

Jaynes, E.T., 1957. Information theory and statistical mechanics. *Physical Review Journals Archive*, 106, 620—630. https://doi.org/10.1103/PhysRev.106.620.

Kadanoff, L.P., 1990. Scaling and universality in statistical physics. *Physica A: Statistical Mechanics and its Applications*, 163, 1—14. https://doi.org/10.1016/0378-4371(90)90309-G.

Kalderon-Asael, B., Katchinoff, J.A.R., Planavsky, N.J., Hood, A.V.S., Dellinger, M., Bellefroid, E.J., Jones, D.S., Hofmann, A., Ossa, F.O., Macdonald, F.A., Wang, C., Isson, T.T., Murphy, J.G., Higgins, J.A., West, A.J., Wallace, M.W., Asael, D., Pogge Von Strandmann, P.A.E., 2021. A lithium-isotope perspective on the evolution of carbon and silicon cycles. *Nature*, 595, 394—398. https://doi.org/10.1038/s41586-021-03612-1.

Kasting, J.F., Howard, M.T., Wallmann, K., Veizer, J., Shields, G., Jaffrés, J., 2006. Paleoclimates, ocean depth, and the oxygen isotopic composition of seawater. *Earth and Planetary Science Letters*, 252, 82—93. https://doi.org/10.1016/j.epsl.2006.09.029.

Katsev, S., Crowe, S.A., 2015. Organic carbon burial efficiencies in sediments: The power law of mineralization revisited. *Geology*, 43, 607—610. https://doi.org/10.1130/G36626.1.

Kipp, M.A., Li, H., Ellwood, M.J., John, S.G., Middag, R., Adkins, J.F., Tissot, F.L.H., 2022. $^{238}U$, $^{235}U$ and $^{234}U$ in seawater and deep-sea corals: A high-precision reappraisal. *Geochimica et Cosmochimica Acta*, 336, 231—248. https://doi.org/10.1016/j.gca.2022.09.018.

Kleidon, A., 2010. A basic introduction to the thermodynamics of the Earth system far from equilibrium and maximum entropy production. *Philosophical Transactions of the Royal Society B: Biological Sciences*, 365, 1303—1315. https://doi.org/10.1098/rstb.2009.0310.

Kleidon, A., Lorenz, R.D., 2005. *Non-equilibrium Thermodynamics and the Production of Entropy. Life, Earth, and Beyond*. Springer, New York.

Lenton, T., Watson, A.J., 2013. *Revolutions that Made the Earth*. Oxford University Press, Oxford.

Lenton, T.M., 1998. Gaia and natural selection. *Nature*, 394, 439—447. https://doi.org/10.1038/28792.

Lovelock, J., 2000. *Gaia: A New Look at Life on Earth*. Oxford University Press, Oxford.

Lyons, T.W., Reinhard, C.T., Planavsky, N.J., 2014. The rise of oxygen in Earth's early ocean and atmosphere. *Nature*, 506, 307—315. https://doi.org/10.1038/nature13068.

Mandelbrot, B.B., 1982. *The Fractal Geometry of Nature*. W.H. Freeman, San Francisco.

Marković, D., Gros, C., 2014. Power laws and self-organized criticality in theory and nature. *Physics Reports*, 536, 41—74. https://doi.org/10.1016/j.physrep.2013.11.002.

Martyushev, L.M., 2010. The maximum entropy production principle: Two basic questions. *Philosophical Transactions of the Royal Society B: Biological Sciences*, 365, 1333—1334. https://doi.org/10.1098/rstb.2009.0295.

Massey, F.J., 1951. The Kolmogorov-Smirnov test for goodness of fit. *Journal of the American Statistical Association*, 46, 68—78. https://doi.org/10.1080/01621459.1951.10500769.

McArthur, J.M., Howarth, R.J., Shields, G.A., Zhou, Y., 2020. Strontium Isotope Stratigraphy. In: *Geologic Time Scale 2020*. Elsevier, pp. 211—238. https://doi.org/10.1016/B978-0-12-824360-2.00007-3.

McInerney, F.A., Wing, S.L., 2011. The Paleocene—Eocene Thermal Maximum: A perturbation of carbon cycle, climate, and biosphere with implications for the future. *Annual Review of Earth and Planetary Sciences*, 39, 489—516. https://doi.org/10.1146/annurev-earth-040610-133431.

Mega, M.S., Allegrini, P., Grigolini, P., Latora, V., Palatella, L., Rapisarda, A., Vinciguerra, S., 2003. Power-law time distribution of large earthquakes. *Physical Review Letters*, 90, 188501. https://doi.org/10.1103/PhysRevLett.90.188501.

Michener, R., Lajtha, K., 2007. *Stable Isotopes in Ecology and Environmental Science*. Wiley-Blackwell, Hoboken. https://doi.org/10.1002/9780470691854.

Middelburg, J.J., 1989. A simple rate model for organic matter decomposition in marine sediments. *Geochimica et Cosmochimica Acta*, 53, 1577—1581. https://doi.org/10.1016/0016-7037(89)90239-1.

Ovtcharova, M., Goudemand, N., Hammer, Ø., Guodun, K., Cordey, F., Galfetti, T., Schaltegger, U., Bucher, H., 2015. Developing a strategy for accurate definition of a geological boundary through radio-isotopic and biochronological dating: The Early—Middle Triassic boundary (South China). *Earth-Science Reviews*, 146, 65—76. https://doi.org/10.1016/j.earscirev.2015.03.006.

Paytan, A., Yao, W., Faul, K.L., Gray, E.T., 2020. Sulfur Isotope Stratigraphy. In: *Geologic Time Scale 2020*. Elsevier, pp. 259—278. https://doi.org/10.1016/B978-0-12-824360-2.00009-7.

Penniston-Dorland, S., Liu, X.-M., Rudnick, R.L., 2017. Lithium isotope geochemistry. *Reviews in Mineralogy and Geochemistry*, 82, 165—217. https://doi.org/10.2138/rmg.2017.82.6.

Present, T.M., Adkins, J.F., Fischer, W.W., 2020. Variability in sulfur isotope records of Phanerozoic seawater sulfate. *Geophysical Research Letters*, 47, e2020GL088766. https://doi.org/10.1029/2020GL088766.

Prigogine, I., 1980. *From Being to Becoming: Time and Complexity in the Physical Sciences*. W. H. Freeman, San Francisco.

Prokoph, A., Shields, G.A., Veizer, J., 2008. Compilation and time-series analysis of a marine carbonate $\delta^{18}O$, $\delta^{13}C$, $^{87}Sr/^{86}Sr$ and $\delta^{34}S$ database through Earth history. *Earth-Science Reviews*, 87, 113—133. https://doi.org/10.1016/j.earscirev.2007.12.003.

Ruppert, D., 2002. Selecting the number of knots for penalized splines. *Journal of Computational & Graphical Statistics*, 11, 735—757. https://doi.org/10.1198/106186002853.

Scholz, C.H., Mandelbrot, B.B., 1989. *Fractals in Geophysics*. Birkhäuser Verlag, Basel. https://doi.org/10.1007/978-3-0348-6389-6.

Schroeder, M.R., 2009. *Fractals, Chaos, Power Laws: Minutes from an Infinite Paradise*. Dover Publications, New York.

Shang, H., 2023a. A generic hierarchical model of organic matter degradation and preservation in aquatic systems. *Communications Earth & Environment*, 4, 16. https://doi.org/10.1038/s43247-022-00667-4.

Shang, H., 2023b. Mineral evolution facilitated Earth's oxidation. *Communications Earth & Environment*, 4, 213. https://doi.org/10.1038/s43247-023-00824-3.

Shang, H., Rothman, D.H., Fournier, G.P., 2022. Oxidative metabolisms catalyzed Earth's oxygenation. *Nature Communications*, 13, 1328. https://doi.org/10.1038/s41467-022-28996-0.

Skilling, J., 1989. Classic Maximum Entropy. In: Skilling, J. (Ed.), *Maximum Entropy and Bayesian Methods*. Springer Netherlands, Dordrecht, pp. 45—52. https://doi.org/10.1007/978-94-015-7860-8_3.

Solow, A.R., 2005. Power laws without complexity. *Ecology Letters*, 8, 361—363. https://doi.org/10.1111/j.1461-0248.2005.00738.x.

Stanley, H.E., Amaral, L.A.N., Gopikrishnan, P., Ivanov, P.C., Keitt, T.H., Plerou, V., 2000. Scale invariance and universality: Organizing principles in complex systems. *Physica A: Statistical Mechanics and its Applications*, 281, 60—68. https://doi.org/10.1016/S0378-4371(00)00195-3.

Tierney, J.E., Zhu, J., Li, M., Ridgwell, A., Hakim, G.J., Poulsen, C.J., Whiteford, R.D.M., Rae, J.W.B., Kump, L.R., 2022. Spatial patterns of climate change across the Paleocene—Eocene Thermal Maximum. *Proceedings of the National Academy of Sciences of the United States of America*, 119, e2205326119. https://doi.org/10.1073/pnas.2205326119.

Vallino, J.J., Algar, C.K., 2016. The thermodynamics of marine biogeochemical cycles: Lotka revisited. *Annual Review of Marine Science*, 8, 333—356. https://doi.org/10.1146/annurev-marine-010814-015843.

Veizer, J., Prokoph, A., 2015. Temperatures and oxygen isotopic composition of Phanerozoic oceans. *Earth-Science Reviews*, 146, 92—104. https://doi.org/10.1016/j.earscirev.2015.03.008.

Vuong, Q.H., 1989. Likelihood ratio tests for model selection and non-nested hypotheses. *Econometrica*, 57, 307. https://doi.org/10.2307/1912557.

Westerhold, T., Marwan, N., Drury, A.J., Liebrand, D., Agnini, C., Anagnostou, E., Barnet, J.S.K., Bohaty, S.M., De Vleeschouwer, D., Florindo, F., Frederichs, T., Hodell, D.A., Holbourn, A.E., Kroon, D., Lauretano, V., Littler, K., Lourens, L.J., Lyle, M., Pälike, H., Röhl, U., Tian, J., Wilkens, R.H., Wilson, P.A., Zachos, J.C., 2020. An astronomically dated record of Earth's climate and its predictability over the last 66 million years.

*Science*, 369, 1383—1387. https://doi.org/10.1126/science.aba6853.

Wu, N., Farquhar, J., Strauss, H., Kim, S.-T., Canfield, D.E., 2010. Evaluating the S-isotope fractionation associated with Phanerozoic pyrite burial. *Geochimica et Cosmochimica Acta*, 74, 2053—2071. https://doi.org/10.1016/j.gca.2009.12.012.

Zhang, F., Lenton, T.M., Del Rey, Á., Romaniello, S.J., Chen, X., Planavsky, N.J., Clarkson, M.O., Dahl, T.W., Lau, K.V., Wang, W., Li, Z., Zhao, M., Isson, T., Algeo, T.J., Anbar, A.D., 2020. Uranium isotopes in marine carbonates as a global ocean paleoredox proxy: A critical review. *Geochimica et Cosmochimica Acta*, 287, 27—49. https://doi.org/10.1016/j.gca.2020.05.011.